doi:10.1093/brain/awz158 BRAIN 2019: 142; 2238–2252 | 2238

BRAIN
A JOURNAL OF NEUROLOGY

Stop-gain mutations in *UBAP1* cause pure autosomal-dominant spastic paraplegia

Xiang Lin,[1,2,*] Hui-Zhen Su,[1,*] En-Lin Dong,[1,*] Xiao-Hong Lin,[1,*] Miao Zhao,[1] Can Yang,[3] Chong Wang,[1] Jie Wang,[3] Yi-Jun Chen,[1] Hongjie Yu,[4] Jianfeng Xu,[4] Li-Xiang Ma,[5] Zhi-Qi Xiong,[3] Ning Wang[1,2] and Wan-Jin Chen[1,2]

*These authors contributed equally to this work.

Hereditary spastic paraplegias refer to a heterogeneous group of neurodegenerative disorders resulting from degeneration of the corticospinal tract. Clinical characterization of patients with hereditary spastic paraplegias represents progressive spasticity, exaggerated reflexes and muscular weakness. Here, to expand on the increasingly broad pools of previously unknown hereditary spastic paraplegia causative genes and subtypes, we performed whole exome sequencing for six affected and two unaffected individuals from two unrelated Chinese families with an autosomal dominant hereditary spastic paraplegia and lacking mutations in known hereditary spastic paraplegia implicated genes. The exome sequencing revealed two stop-gain mutations, c.247_248insGTGAATTC (p.I83Sfs*11) and c.526G>T (p.E176*), in the ubiquitin-associated protein 1 (*UBAP1*) gene, which co-segregated with the spastic paraplegia. We also identified two *UBAP1* frameshift mutations, c.324_325delCA (p.H108Qfs*10) and c.425_426delAG (p.K143Sfs*15), in two unrelated families from an additional 38 Chinese pedigrees with autosomal dominant hereditary spastic paraplegias and lacking mutations in known causative genes. The primary disease presentation was a pure lower limb predominant spastic paraplegia. *In vivo* downregulation of Ubap1 in zebrafish causes abnormal organismal morphology, inhibited motor neuron outgrowth, decreased mobility, and shorter lifespan. UBAP1 is incorporated into endosomal sorting complexes required for transport complex I and binds ubiquitin to function in endosome sorting. Patient-derived truncated form(s) of UBAP1 cause aberrant endosome clustering, pronounced endosome enlargement, and cytoplasmic accumulation of ubiquitinated proteins in HeLa cells and wild-type mouse cortical neuron cultures. Biochemical and immunocytochemical experiments in cultured cortical neurons derived from transgenic *Ubap1*^{flox} mice confirmed that disruption of UBAP1 leads to dysregulation of both early endosome processing and ubiquitinated protein sorting. Strikingly, deletion of *Ubap1* promotes neurodegeneration, potentially mediated by apoptosis. Our study provides genetic and biochemical evidence that mutations in *UBAP1* can cause pure autosomal dominant spastic paraplegia.

1 Department of Neurology and Institute of Neurology, The First Affiliated Hospital of Fujian Medical University, Fuzhou 350005, China
2 Fujian Key Laboratory of Molecular Neurology, Fujian Medical University, Fuzhou 350005, China
3 Institute of Neuroscience and State Key Laboratory of Neuroscience, CAS Center for Excellence in Brain Science and Intelligence Technology, Shanghai Institutes for Biological Sciences, Chinese Academy of Sciences, Shanghai 200031, China
4 Program for Personalized Cancer Care, NorthShore University HealthSystem, Evanston, IL 60201, USA
5 Department of Anatomy, Histology and Embryology, Shanghai Medical College, Fudan University, Shanghai 200032, China

Correspondence to: Wan-Jin Chen
Department of Neurology and Institute of Neurology, The First Affiliated Hospital of Fujian Medical University, Fuzhou 350005, China
E-mail: wanjinchen75@fjmu.edu.cn

Received November 1, 2018. Revised March 14, 2019. Accepted April 15, 2019. Advance Access publication June 15, 2019

Keywords: hereditary spastic paraplegia; ubiquitin-associated protein 1; early endosome; ubiquitination; neurodegeneration

Abbreviations: ESCRT = endosomal sorting complexes required for transport; HSP = hereditary spastic paraplegia; MO = morpholino oligomer; MVB = multivesicular body; SOUBA = solenoid of overlapping UBAs domain

Introduction

Hereditary spastic paraplegias (HSP) are a highly heterogeneous group of neurodegenerative disorders affecting the corticospinal tract, with an estimated prevalence of 2–10 in 100 000 individuals (Ruano *et al.*, 2014; Kara *et al.*, 2016). Clinically, HSP is typically classified into one of two types: a pure form and a complicated form. Pure HSP includes progressive lower limb spasticity and weakness, while complicated HSP is accompanied by neurological or other features (Zempel *et al.*, 2015; Dong *et al.*, 2018). Notoriously, HSP is characterized by great heterogeneity in inheritance, with known instances including autosomal dominant, autosomal recessive, X-linked, and even mitochondrial inheritance (Coutelier *et al.*, 2015).

Over the past two decades, more than 70 HSP disease-causing genes have been identified, enabling distinction of genetic subtypes (Estrada-Cuzcano *et al.*, 2017). Despite these advances, no genetic diagnosis exists for ~50% of HSP patients. Clearly, mutations in unidentified genes give rise to many HSP cases, compounding the limited foundational understanding of the pathophysiological basis underlying the constellation of neurodegenerative diseases that are currently conceptualized as HSP. Nevertheless, discovery of functional overlap among HSP-associated genes has led to recent hypotheses for possible common pathogenic mechanisms connecting the diverse array of known causative mutations, supported by direct evidence of oxidative stress, axonal transport, lipid metabolism, and autophagy, among others (Fink, 2013; Lo Giudice *et al.*, 2014).

Previous studies have also linked HSP to the endosomal sorting complex required for the ESCRT (endosomal sorting complexes required for transport) transport system. There are four multi-subunit ESCRT complexes (0–III) that function in the maturation of multivesicular bodies (MVBs) and in the recognition and sorting of ubiquitinated protein into various cellular vesicles (Raiborg *et al.*, 2009). Some ESCRT complex subunits participate in the maintenance of healthy neuronal structure and function (Sweeney *et al.*, 2006; Loncle *et al.*, 2015; Sheehan *et al.*, 2016). Moreover, the dysfunction of multiple ESCRT complex subunits has been implicated in multiple neurodegeneration diseases. For example, mutations in CHMP2B—a subunit of ESCRT-III—have been linked with frontotemporal dementia and amyotrophic lateral sclerosis (Skibinski *et al.*, 2005; Parkinson *et al.*, 2006), and neurons lacking the ESCRT-III subunit Snf7 present with accumulation of an amyloid precursor protein implicated in Alzheimer's disease (Lee and Gao, 2012). Mutation in a subunit of the ESCRT-I complex—VPS37A—has previously been shown to cause a form of HSP (Zivony-Elboum *et al.*, 2012).

Here, whole exome sequencing revealed that four unrelated pure autosomal-dominant HSP families commonly carried stop-gain mutations in the fourth exon of the gene encoding the ESCRT-I complex subunit ubiquitin-associated protein 1 (UBAP1). We confirmed that these mutated alleles did indeed produce truncated *UBAP1* gene products and characterized to the disease features and genetic variation of patients and relatives in the four HSP families. We subsequently performed a series of biochemical and cell biology functional studies in human cells, zebrafish larvae, and in cultured cortical neurons derived from the wild-type mouse and a transgenic *Ubap1*^{flox} mouse line that we developed. Our biochemical and cell biology evidence collectively points to a dominant-negative pathomechanism in which the truncated gene products from the disease alleles dysregulate endosomal processing and ubiquitinated protein sorting, thereby promoting neurodegeneration, potentially as mediated by apoptosis.

Materials and methods

Subject recruitment and sample collection

A cohort of HSP patients from 112 families were recruited by the Department of Neurology of the First Affiliated Hospital of Fujian Medical University. All patients fulfilling the Harding's classification for HSP were enrolled, irrespective of their genetic diagnosis (Harding, 1983). For HSP families, we also included other available unaffected relatives. In addition, 500 unrelated healthy ethnically matched individuals were selected and used as the control group. Genomic DNA of all participants was extracted from peripheral blood leucocytes using QIAamp DNA Blood Mini Kits (QIAGEN).

Informed written consent was obtained from all the participants according to the Declaration of Helsinki. This study was approved by the Ethics Committee of the First Affiliated Hospital of Fujian Medical University (FYYY2006–01–19–01).

Sequencing and data analysis

Next-generation sequencing was carried out to help identify causative genes in the HSP patients: we used a panel of targeted exome sequencing to screen mutations in 79 previously reported HSP-related genes. For families without mutations in known HSP-causative genes, we selected particularly symptomatic family members when possible to perform whole exome sequencing using an Agilent SureSelect All Exon 50MB (V6) capture kit. The captured reads were sequenced on the

Illumina HiSeq 3000 platform. We used Burrows-Wheeler Aligner-mem software package to align the reads to human genome build 38. Variants were called using the Genome Analysis Toolkit and annotated with ANNOVARA.

Identified genetic variants that were characterized by any of the two following criteria were excluded from further analysis: (i) the variant did not affect the amino acid sequence; and (ii) the allele frequency was >1% in the 1000 Genomes Project dataset, the NHLBI Exome Sequencing Project dataset, or the genome Aggregation Database. Finally, we screened possible disease-causing genes assuming a dominant inheritance mode and based on the co-segregation of mutations with the disease phenotypes.

Sanger sequencing

Sanger sequencing was performed on the coding region of the *UBAP1* by using an ABI 3700 automated sequencer (Applied Biosystems). The specific primer sequences are listed in Supplementary Table 1. Sequencing results were analysed with Chromas software (Technelysium Pty Ltd).

Genetic linkage analysis

Linkage analyses were performed using GeneHunter software (Kruglyak *et al.*, 1996). For the disease locus, an autosomal dominant mode of inheritance was assumed: the disease allele frequency was set at 0.00001 to reflect the occurrence rate of 1 in 150 000. The penetrance of carriers and non-carriers was set at 0.95 and 0, respectively. This model was based on an assumption of a highly penetrant HSP mutation with no phenocopy. For the marker locus, any pathogenic *UBAP1* mutation was coded as 1, otherwise, 0.

Zebrafish growth, microinjection and behavioural analysis

Zebrafish were maintained as previously described at Shanghai Model Organisms Center, Inc., (Ohki *et al.*, 2017). They were allowed to develop at 28.5°C and were staged by hours or days after fertilization under standard conditions. The establishment and characterization of the *hb9*:GFP transgenic lines followed previously described methods (Kanungo *et al.*, 2011). The three different morpholino oligomers (MOs) targeting the zebrafish *ubap1* orthologue (NP_001315273) were synthesized by Gene Tools (Philomath) (Supplementary Table 1), and were used as follows: an MO with a sequence unrelated *ubap1* (control-MO), an MO that targeted a splicing site between intron 2 and exon 3 of *ubap1* in an antisense orientation (I2E3-MO), and an MO that targeted the *ubap1* translation initiation site in an antisense orientation (ATG-MO); these were microinjected into fertilized one-cell stage embryos according to standard protocols (4 ng per embryo was used for each injection).

To evaluate escape responses, 48 h post-fertilization zebrafish larvae after the MO injection were touched with the tip of a fine needle at least twice at the dorsal tip of the tail or trunk; at least 50 fish were assayed for each genotype. When a morphant did not move a distance of at least three times its own body length upon touching, this was considered to be a mobility defect. We also recorded videos. To assess spinal motor neuron formation in morphants, the *hb9*:GFP embryos were dechorionated and anaesthetized with 0.016% tricaine methanesulphonate (MS-222, Sigma-Aldrich) at 48 h post-fertilization. The morphants were then oriented on a lateral side (anterior, left; posterior, right; dorsal, top) or dorsal side, and mounted with 3% methylcellulose in a depression slide for observation by fluorescence microscopy (Nikon SMZ 1500). The phenotypes of spinal motor neurons were quantitatively analysed using image-based morphometric analysis (NIS-Elements D3.1) and ImageJ software.

DNA constructs

All the plasmids used in this study are listed in Supplementary Table 2. To generate the plasmids for each of the *UBAP1* truncation mutant alleles, a Mut Express® II Fast Mutagenesis Kit V2 (Vazyme) was used according to the manufacturer's instructions.

HEK293T and HeLa cell culture and transfection

The HEK293T and HeLa cells lines were both from Cell Bank, Type Culture Collection, of the Chinese Academy of Sciences (CBTCCCAS). These two cell lines were tested for mycoplasma contamination, and were authenticated by the supplier (Supplementary Fig. 1). The cells were incubated in high glucose Dulbecco's modified Eagle medium (DMEM) supplemented with 10% foetal bovine serum (FBS) and maintained at 37°C under 5% CO_2. Transient transfection of HEK 293T or HeLa cells with wild-type or mutated-UBAP1 plasmids was performed using Lipofectamine® 3000 (Thermo). Following transfection, cells were cultured for an additional 24 h before harvesting for immunoblotting (in HEK 293T cells) or staining for imaging analysis (in HeLa cells) (Supplementary Table 3).

Co-immunoprecipitation

HEK293T cells were co-transfected with HA-tagged *TSG101*, HA-tagged *VPS28*, GFP-tagged *VPS37A*, and with or without wild-type or mutant flag-tagged *UBAP1* using Lipofectamine® 3000 (Thermo) according to the manufacturer's instructions. After 24 h, cells were lysed and cleared by centrifugation. Protein A agarose beads (50% working dilution, Sigma Aldrich) were incubated with the cleared lysates. The bound proteins were then eluted by 2× reducing SDS loading buffer, resolved by 10% SDS-PAGE gels, and immunoblotted with the antibodies listed in Supplementary Table 3.

Generation of transgenic *Ubap1*^{flox} mice

All of the experiments involving the use of mice were conducted in accordance with the Animal Care and Use Committee of the Institute of Neuroscience of the Chinese Academy of Sciences. The transgenic *Ubap1*^{flox} mice that we generated had the *Ubap1* locus exon 3 flanked by two loxP sites: 5′ loxP inserted into intron 2 at chromosome 4 (41371239) and 3′ loxP inserted into intron 3 at chromosome 4 (41372138). Briefly, we constructed the pU6-sgRNA-Cas9 vector targeting the *Ubap1* locus and the pU6-loxP-*Ubap1*-loxP vector was used as the template for

homologous recombination (Supplementary Table 1). Both transgenic vectors were linearized and purified for co-microinjection into mouse zygotes, which were obtained by mating of C57BL/6 J males with superovulated C57BL/6 J females. Injected zygotes were transferred into pseudopregnant female mice. Each of the 5′ or 3′ loxP sites in the resulting mouse line were identified by PCR (Supplementary Table 1). Southern blotting was used to further confirm successful homologous recombination at both the 5′ and 3′ loxP sites in the F1 mice. All of the homozygous *Ubap1*$^{flox/flox}$ mice were generated by mating male and female heterozygous *Ubap1*^{flox}.

Primary cortical neurons culture and electroporation

Cortices were dissected from postnatal Day 0 (P0) wild-type and *Ubap1*$^{flox/flox}$ mouse pups, then the primary cortical neurons were prepared as described previously (Söllvander *et al.*, 2016). Neurons were electrotransfected with vectors using an Amaxa Nucleofector^{TM} system (Lonza). For the conditional deletion *Ubap1* experiments, neurons were co-transfected with a plasmid bearing Cre-T2A-EGFP or Cre-Myc construct that facilitated identification of successful Cre recombination activity and a plasmid bearing an EEA1-Flag construct to label early endosomes. For the rescue assay, the neurons were co-transfected with one of three additional plasmids bearing for full-length human UBAP1 (UBAP1$^{full\text{-}length}$), truncated mutant variant of UBAP1 (UBAP1^{K143fs}), or the control CAG-EGFP constructs. For the overexpression assay, neurons were co-transfected with a plasmid bearing UBAP1$^{full\text{-}length}$ or UBAP1^{K143fs} construct, and a plasmid bearing an EEA1-Flag.

Immunocytochemistry and quantification

Immunostaining was carried out as described previously (Dong *et al.*, 2018). The primary antibodies used are listed in Supplementary Table 3. Images were acquired using a Leica SP-8 confocal microscope. Images of each individual group were captured using identical microscope, laser, filter, and camera settings. ImageJ software was used for the measurement of the early endosome diameters, and the fluorescent ubiquitin signals, which were normalized to their own soma size.

Western blotting

The cells were harvested in the cell lysis reagent supplemented with protease inhibitor cocktail, and the lysates were cleared by centrifugation at 14 000 *g* for 20 min. Protein extracts were separated on 10% SDS-PAGE gels and then immunoblotted with the primary antibodies listed in Supplementary Table 3. HRP-conjugated secondary antibodies (1:5000, Santa Cruz) were used to detect primary antibodies and proteins were visualized by chemiluminescence (Beyotime).

Statistical analyses

Data are presented as mean ± standard error of mean (SEM). Kaplan-Meier survival data were analysed with the program GraphPad Prism. Statistical significance was assessed by one-way analysis of variance (ANOVA) followed by Bonferroni or Dunnett T3 *post hoc* tests. Differences were considered statistically significant when $^{*}P < 0.05$, $^{**}P < 0.01$, $^{***}P < 0.001$, or $^{***}P < 0.0001$.

Data availability

The datasets generated during and/or analysed during the current study are available from the corresponding author on reasonable request.

Results

Identification of stop-gain mutations in *UBAP1* in four unrelated autosomal dominant HSP families

We recruited 112 HSP families and initially performed targeted sequencing of 79 known HSP-causative genes. This analysis identified pathogenic mutations in 74 (66.1%) of the families (Supplementary Table 4). Seeking to systematically identify the causal genes for the pedigrees lacking known mutations, we performed whole exome sequencing of four patients with spastic paraplegia phenotypes (Patients I1, II1, II2, and III1) and one unaffected individual (Subject III2) from a three-generation pedigree (Family 1, Fig. 1A). We assumed a dominant disease model and therefore focused on candidate genes that met the following criteria: (i) heterozygous variants; that were (ii) located in gene coding regions; (iii) not yet reported in public databases (dbSNP, the 1000 Genome Project, and the genome Aggregation Database); and (iv) that were shared by all patients but not by the unaffected family member. This strategy identified five heterozygous mutations in candidate HSP-causative genes: *UBAP1* (c.247_248insGTGAATTC), *ARMC12* (c.274C>T), *CRISP2* (c.320G>C), *ZNF735* (c.1010C>T), and *DNAH1* (c.2391+5g>a) (Supplementary Table 5).

Further, to study a second family with disease manifestations consistent with a dominant mode of inheritance, we also performed whole exome sequencing for a proband (Patient III1), her affected mother (Patient II4), and her unaffected aunt (Subject II5) (Family 2, Fig. 1B). We used the aforementioned search criteria and identified 41 genes with candidate HSP-causative mutations in Family 2 (Supplementary Table 6). Subsequently, comparison of the candidate genes identified in these separate analyses revealed that *UBAP1* was the only gene implicated in both Families 1 and 2. To identify additional deleterious variants in *UBAP1*, we then performed Sanger sequencing of the entire coding regions and the intron-exon boundaries of the *UBAP1* loci (containing seven exons) in probands from the remaining 38 HSP families. Two additional heterozygous mutations of *UBAP1* were found in two other additional probands: c.425_426delAG in Family 3 (Fig. 1C), and c.324_325delCA in Family 4 (Fig. 1D).

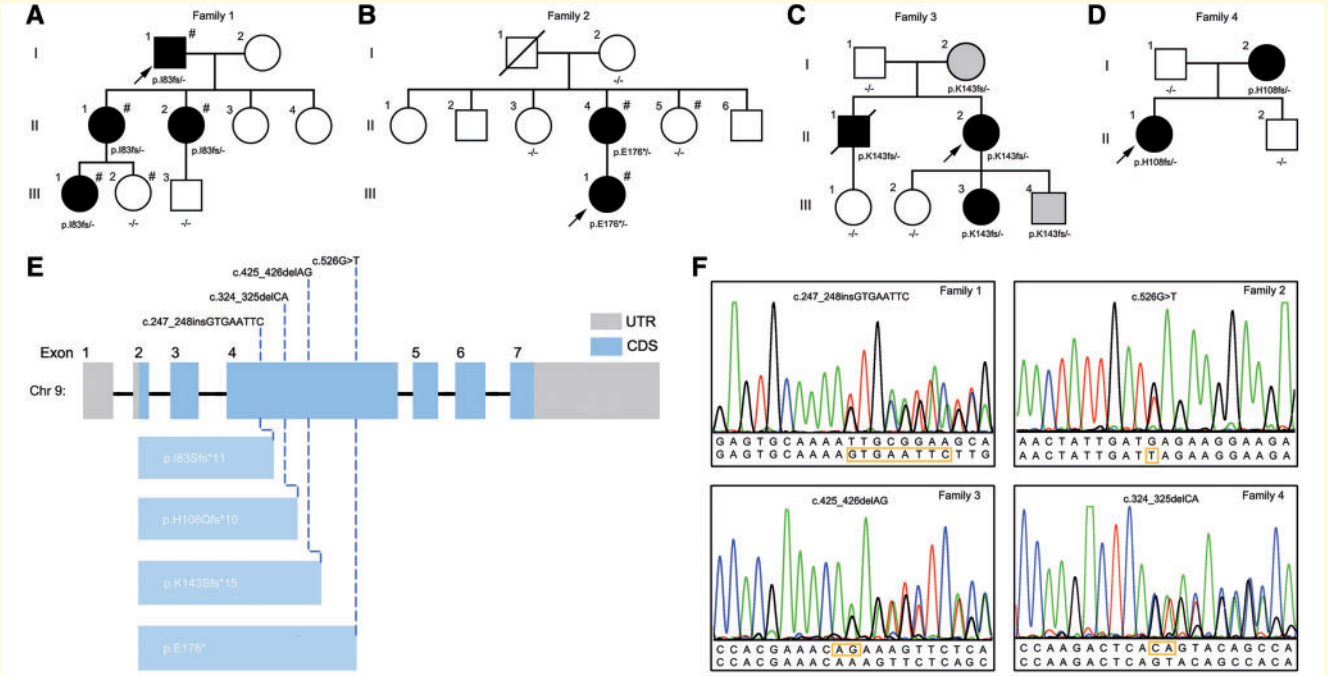

Figure 1 Stop-gain mutations occur in the *UBAP1* gene in four unrelated autosomal dominant HSP families. (**A**–**D**) The pedigrees of HSP Families 1 (**A**), 2 (**B**), 3 (**C**), and 4 (**D**), with *UBAP1* mutations indicated. Filled black squares and circles indicate unambiguously affected individuals, grey squares and circles indicate largely asymptomatic individuals. The proband in each family is indicated by an arrow. The genotypes of all available family members were determined. Dash symbol indicates reference allele; hash symbol indicates individuals selected for whole-exome sequencing. (**E**) Schematic diagram of the four mutations at the *UBAP1* locus, and the truncated mutant variant forms of UBAP1 that these alleles encode. (**F**) Sanger sequencing results for four mutations of *UBAP1* gene in four unrelated HSP families. The marked sequences (yellow boxes) indicate the position of the mutation. See Table 1 for LOD scores from a two-point linkage analysis under different θ-values in four unrelated HSP families that all exhibit mutations in *UBAP1*.

Strikingly, all four of these mutations (p.I83Sfs*11 in Family 1, p.E176* in Family 2, p.K143Sfs*15 in Family 3, and p.H108Qfs*10 in Family 4) were stop-gain mutations in exon 4 that apparently result in the expression of truncated variants of the UBAP1 protein (Fig. 1E).

To assess the co-segregation of *UBAP1* mutations with the spastic paraplegia disease phenotype, we Sanger sequenced the *UBAP1* loci of all members of these four families whose DNA samples were available, and then performed a two-point genetic linkage analysis. For the disease locus, an autosomal dominant mode of inheritance was assumed: the disease allele frequency was 0.00001, and penetrance of carriers and non-carriers was set at 0.95 and 0, respectively. For the marker locus, any pathogenic *UBAP1* mutation was coded as 1, otherwise, 0. This revealed complete co-segregation between the spastic paraplegia phenotype and the *UBAP1* mutations, with a total logarithm of odds (LOD) score of 3.876 for the zero-recombination fraction (Table 1).

To evaluate the frequency of these four stop-gain mutations in the general population, we performed Sanger sequencing on samples from 500 healthy ethnically matched individuals and did not find a single instance of these mutations from these controls. We next looked for additional variants within the entire coding regions, untranslated regions, and the intron-exon boundaries of *UBAP1* in 100 control subjects. Three known heterozygous or homozygous variants, c.1189G>A, c.1368+159g>a, and c.2157G>C (Supplementary Table 7), were found and classified as benign variants according to the standards and guidelines for the interpretation of sequence variants (Richards *et al.*, 2015). Collectively, these results strongly suggest that the four heterozygous stop-gain mutations that we identified in *UBAP1* cause autosomal dominant HSP.

Clinical characterization in HSP patients with *UBAP1* mutations

The four families with the stop-gain mutations in *UBAP1* exon 4 clearly exhibited a pattern of autosomal dominant inheritance, albeit with incomplete penetrance (Family 3, Fig. 1C); the clinical characteristics of all 13 patients are summarized in Table 2. Fundamentally, all of these patients presented as pure HSP; further, we did not detect any UBAP1-specific clinical features that distinguished it from typical HSP subtypes SPG4 or SPG3A.

The four families showed a highly variable age of onset (6 to 61 years) and an apparent intrafamilial phenotypic variation between affected members. The proband (Patient I1) of Family 1 first experienced toe-walking at age 43.

Table 1 LOD scores from a two-point linkage analysis under different θ values in four unrelated HSP families that all exhibit mutations in *UBAP1*

θ-values	0.00	0.01	0.02	0.05	0.10	0.20	0.30	0.40	0.50
Family 1	1.189	1.167	1.145	1.079	0.967	0.734	0.494	0.249	0.000
Family 2	0.894	0.877	0.859	0.805	0.713	0.515	0.311	0.125	0.000
Family 3	1.492	1.466	1.440	1.360	1.224	0.941	0.642	0.330	0.000
Family 4	0.301	0.292	0.284	0.258	0.215	0.133	0.064	0.017	0.000
Total LOD scores	**3.876**	3.802	3.728	3.502	3.119	2.323	1.511	0.721	0.000

Value in bold indicates a total LOD score for the zero recombination fraction in four unrelated HSP families.

Table 2 A summary of clinical features in patients with *UBAP1* mutations

	Family 1				Family 2		Family 3					Family 4	
Patient	**I 1**	**II 1**	**II 2**	**III 1**	**II 4**	**III 1**	**I 2**	**II 1**	**II 2**	**III3**	**III 4**	**I 2**	**II 1**
Sex	M	F	F	F	F	F	F	M	F	F	M	F	F
AAO	43	16	16	10	10	10	61	12	15	10	8	10	6
Duration	20	31	26	14	38	12	0	22	22	2	0	26	7
Disability score	3	2	2	2	3	2	1	3	2	2	1	3	2
LL hypermyotonia	+	+	+	+	+	+	–	+	+	+	–	+	+
LL hyperreflexia	+	+	+	+	+	+	+	+	+	+	+	+	+
Babinski sign	+	+	+	+	+	+	–	+	+	+	–	+	+
LL atrophy	–	–	–	–	–	–	–	–	–	–	–	–	–
Pes cavus	–	–	–	–	+	–	–	+	+	–	–	–	–
Ankle clonus	+	+	+	+	–	–	–	+	+	+	–	+	+
Sphincter disturbance	+	–	–	–	–	–	–	–	–	–	–	–	–
Cognitive impairment	–	–	–	–	–	–	–	–	–	–	–	–	–
Ataxia	–	–	–	–	–	–	–	–	–	–	–	–	–
Dysarthria	–	–	–	–	–	–	–	–	–	–	–	–	–
Brain MRI[a]	Normal	Normal	Normal	Normal	Normal	Normal	Normal	Normal	Normal	Normal	Normal	Normal	Normal
Spine MRI[b]	Normal	Normal	Normal	Normal	Normal	Normal	NA	NA	NA	NA	NA	Normal	Normal
Electromyogram[c]	Normal	Normal	Normal	Normal	Normal	Normal	NA	NA	NA	NA	NA	Normal	Normal
Serum creatine kinase, IU/l	108	33	51.7	84.0	138	72	NA	NA	NA	NA	NA	83	110

AAO = age at onset; F = female; LL = lower limbs; M = male; NA = not available + = present; – = absent.
Disability score: 1 = normal, 2 = walks but cannot run, 3 = walks with aids, 4 = wheelchair bound.
[a]Brain MRIs was acquired using sagittal T_1 (section thickness = 3 mm) and axial T_2 (slice thickness = 5 mm).
[b]Cervical, thoracic and lumbar spinal cord MRIs were acquired on the same scanner (sagittal T_1 and T_2, slice thickness = 3 mm; axial T_1 and T_2, slice thickness = 4 mm).
[c]Motor conduction velocities (MCVs) were performed.

Following a 20-year history of spastic paraplegia, he had difficulties walking, accompanied by progressive sphincter disturbance. Other subjects (Patients II1, II2 and III1) were younger at onset, and except sphincter disturbances, presented similar clinical courses for the disease. Detailed neurological examination revealed consistent phenotypes among Family 1 patients, including hypermyotonia, hyperreflexia, Babinski sign, and ankle clonus. Proband (Patient III1) of Family 2 and her affected mother (Patient II4) presented with childhood-onset abnormal gait and typical signs of pure spastic paraplegia (spasticity, hyperreflexia, and Babinski sign); the mother (Patient II4) also suffered from *pes cavus*.

The proband (Patient II2) of Family 3 initially presented with gait difficulties and *pes cavus* at age 15, but had no obvious progression since onset. Her twin brother (Patient II1) presented with similar symptoms and signs, but died of an unrelated cause at age 34. The 12-year-old daughter (Patient III3) of Patient II2 showed typical signs of pure spastic paraplegia. Notably, the 8-year-old son (Patient III4) and 61-year-old mother (Patient I2) of Patient II2 were largely asymptomatic, only exhibiting hyperreflexia in their lower limbs with subtle gait changes. Family 4 proband (Patient II1) and her affected mother (Patient I2) presented with childhood-onset abnormal gait and showed typical signs of pure spastic paraplegia and ankle clonus. Moreover, all the available patients did not exhibit additional complicated signs (e.g. muscle atrophy, cognitive impairment, ataxia, or dysarthria), and no positive changes were detected in brain and spine MRI, electromyography, and serum creatine kinase evaluations. Thus, all HSP patients carrying *UBAP1* mu-

tations could be classified as having pure HSP according to Harding's guidelines for clinical manifestation (Harding, 1983).

Knockdown of ubap1 causes zebrafish larvae inhibited motor neuron outgrowth and decreased mobility

UBAP1 is highly conserved among animal species, and analysis using the expression tools at the BioGPS database showed a ubiquitously distributed expression pattern for UBAP1 (Supplementary Fig. 2) in human, mouse and zebrafish (*Danio rerio*). Transgenic zebrafish have been widely used with a motor neuron-specific *hb9* promoter and *GFP*-reporter-construct to study neurodegenerative diseases, including HSP (Kozol *et al.*, 2016). We used two types of MOs (splice blocking: I2E3-MO and translational blocking: ATG-MO) to successfully knockdown ubap1 *hb9:GFP* zebrafish (Supplementary Fig. 3A and B).

We noted that zebrafish injected with control-MO at 2 days post-fertilization (dpf) have straight bodies (Fig. 2A and B) and distinct chevron-shaped somites (Fig. 2C). However, the morphants injected with the MOs targeting ubap1 expression (I2E3-MO or ATG-MO) exhibited a highly penetrant phenotype characterized by ventral body curvature (Fig. 2 A and B) and U-shaped somites (Fig. 2C) that could first be seen at 24 h post-fertilization (30 somite stage). We next examined spinal motor axonal phenotypes and found that, compared to larvae injected with control-MO, the morphants exhibited shorter axonal length (Fig. 2D and E), indicating that ubap1 functions in the outgrowth of motor axons. We then conducted touch behavioural assays to assess movement, which revealed that morphants, but not controls, had significant defects in larval mobility (Fig. 2F, G and Supplementary Video 1), suggesting that ubap1's contribution to motor neuron development and/or function is required for normal behaviours in zebrafish.

We also examined fish survival for 10 dpf and generated Kaplan-Meier survival curves, which indicated that the median lifespans of morphants (I2E3-MO, 6 days; ATG-MO, 1 day) were both significantly shorter than the control (>10 days) (Fig. 2H and Supplementary Fig. 3C). Importantly, the phenotypes we observed following the disruption of ubap1 expression are quite similar to multiple phenotypes observed in previous studies of zebrafish, which explored the functional contribution of HSP-causative genes (*SPAST*, *PNPLA6* and *GBA1*) in motor neurons (Martin *et al.*, 2013; Song *et al.*, 2013; Jardin *et al.*, 2018). Thus, our results from genetic knockdown experiments in zebrafish further support that mutations in *UBAP1* can cause deleterious effects in neurons that are relevant to the pathogenesis of autosomal dominant HSP.

Truncated UBAP1 impairs endosomal ubiquitin processing but not interaction with ESCRT-I subunits

The human gene *UBAP1*, previously known as *NAG20*, encodes a 502 amino acid (aa) protein. Biochemically, the UBAP1 protein is relatively well studied and is known to have at least three functional motifs: an N-terminal UBAP1-MVB12-associated (UMA) domain (17–63 aa), a HIS-domain protein tyrosine phosphatase (HD-PTP) binding region (260–269 aa), and a C-terminal solenoid of overlapping UBAs (SOUBA) domain (390–500 aa) (Stefani *et al.*, 2011; Gahloth *et al.*, 2016). Recall that each of the four stop-gain mutations identified in the HSP families in the present study were distributed exclusively within exon 4 of the *UBAP1* locus (Fig. 1E); therefore, each mutation is expected to result in the production of a truncated mutant form of UBAP1 that lacks the HD-PTP binding region and the SOUBA domain. Immunoblotting analysis confirmed that each of the four mutations did indeed result in the production of truncated mutant forms of UBAP1 (Supplementary Fig. 4A).

Previous functional studies have demonstrated that UBAP1's UMA domain functions in its interaction with the central stalk region of the ESCRT-I complex (Agromayor *et al.*, 2012; Wunderley *et al.*, 2014). To determine whether the truncated UBAP1 mutants still retain their ability to physically interact with the other members of the ESCRT-I complex, we co-expressed various ESCRT-I subunits (VPS37A, TSG101, and VPS28) alongside either full-length UBAP1 or each of the truncated UBAP1 variants in HEK 293T cells. Our co-immunoprecipitation assays revealed that full-length UBAP1 and all four of the mutants were able to interact with each of the ESCRT-I subunits, and no such interactions were detected for samples lacking the Flag-UBAP1 variant (Fig. 3A); quantification of these interactions revealed no significant difference in binding amongst the full-length and truncation mutant forms of UBAP1 (Fig. 3B–D). Thus, any pathogenic influence of these truncating mutations does not obviously result from the disruption of UBAP1's binding with other members of the ESCRT-I complex.

Previous studies have reported critical roles for both the HD-PTP binding region and the SOUBA domain in ubiquitin homeostasis during early endosome processing; these studies showed that siRNA-mediated knockdown UBAP1 in HeLa cells (i) caused clustering/aggregation of early endosomes; and (ii) caused dramatic accumulation of ubiquitinated proteins (note that knockdown of the HD-PTP-binding-region-interaction partner HDPTP was also reported to cause these two phenotypes) (Stefani *et al.*, 2011). To investigate possible functional consequences of the stop-gain *UBAP1* mutations identified in the HSP families, we overexpressed the full-length or truncation mutant forms of UBAP1 in HeLa cells. Consistent with essential functional roles for both the HD-PTP binding

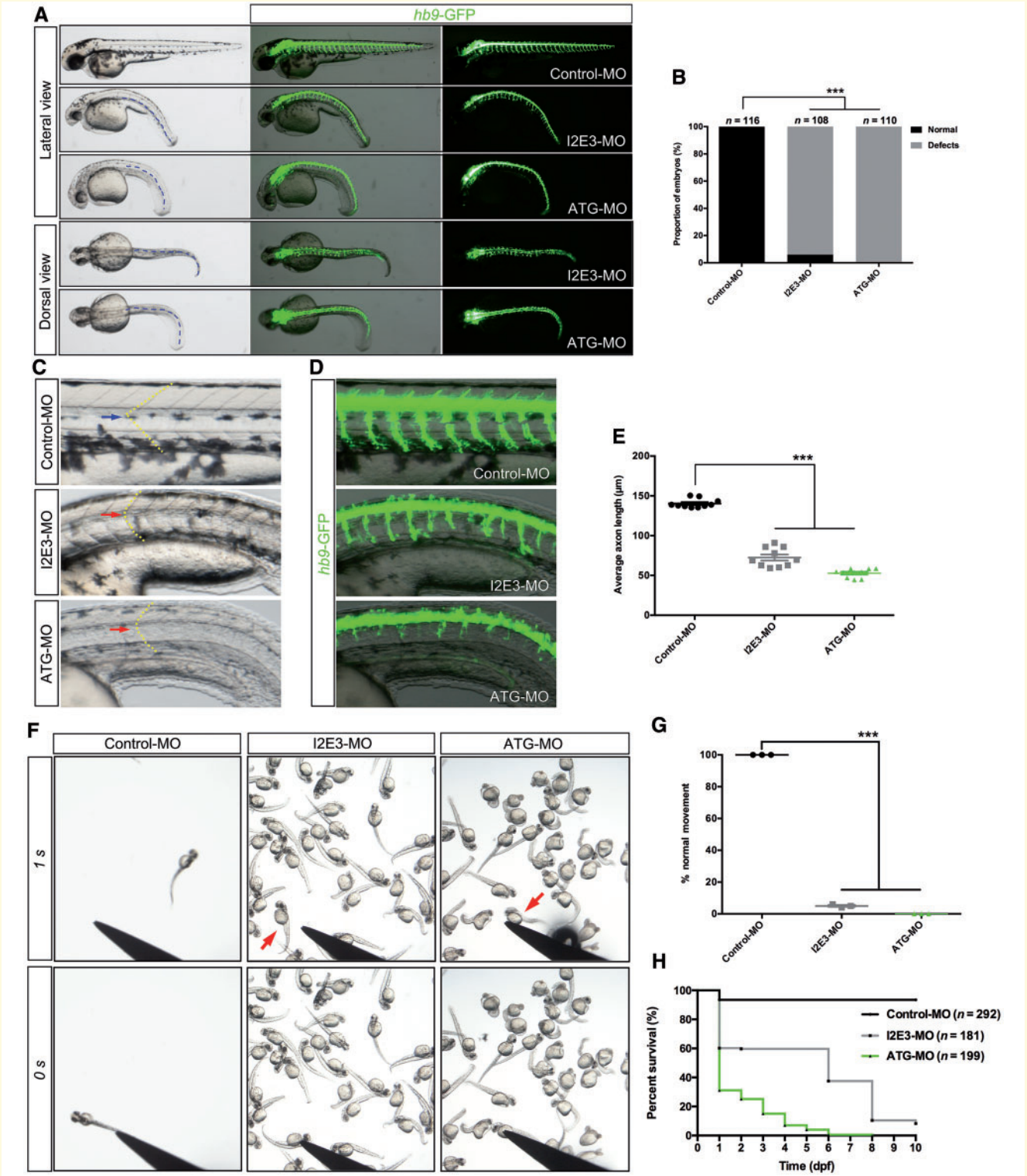

Figure 2 Functional characterization of *ubap1* in *hb9:GFP* zebrafish (*D. rerio*). (**A**–**C**) Gross morphology of *hb9:GFP* zebrafish embryos at 2 dpf. Knockdown of Ubap1 presents ventral body curvature (**A**, blue dotted line) and U-shaped somites (**C**, red arrow), compared with control-MO (**C**, blue arrow, chevron-shaped somites). (**B**) The percentage of embryos with development defects (n = ~110 fish/per group). (**D**) Image of trunk regions taken at 2 dpf, with the spinal motor neuron structures visualized by GFP fluorescence, indicating the impaired motor axon growth in knockdown ubap1 morphants. (**E**) Measurement of the average motor axon length, revealing the significant shorter axons in the knockdown Ubap1 morphants (n = 10 zebrafish/group, with ~30 axons examined per fish). (**F** and **G**) The stereotypic escape response assays revealing the significant mobility defect of knockdown ubap1 morphants at 2 dpf (see Supplementary Video 1; n = ~100 fish/group, with fish pooled from three clutches). (**H**) Kaplan-Meier survival curves for survival in control versus knockdown Ubap1 morphants over a 10-day period (n = more than 180 fish/group; Supplementary Fig. 3). $P < 0.0001$, log-rank test. Error bars indicate means ± SEM. ***$P < 0.001$, one-way ANOVA.

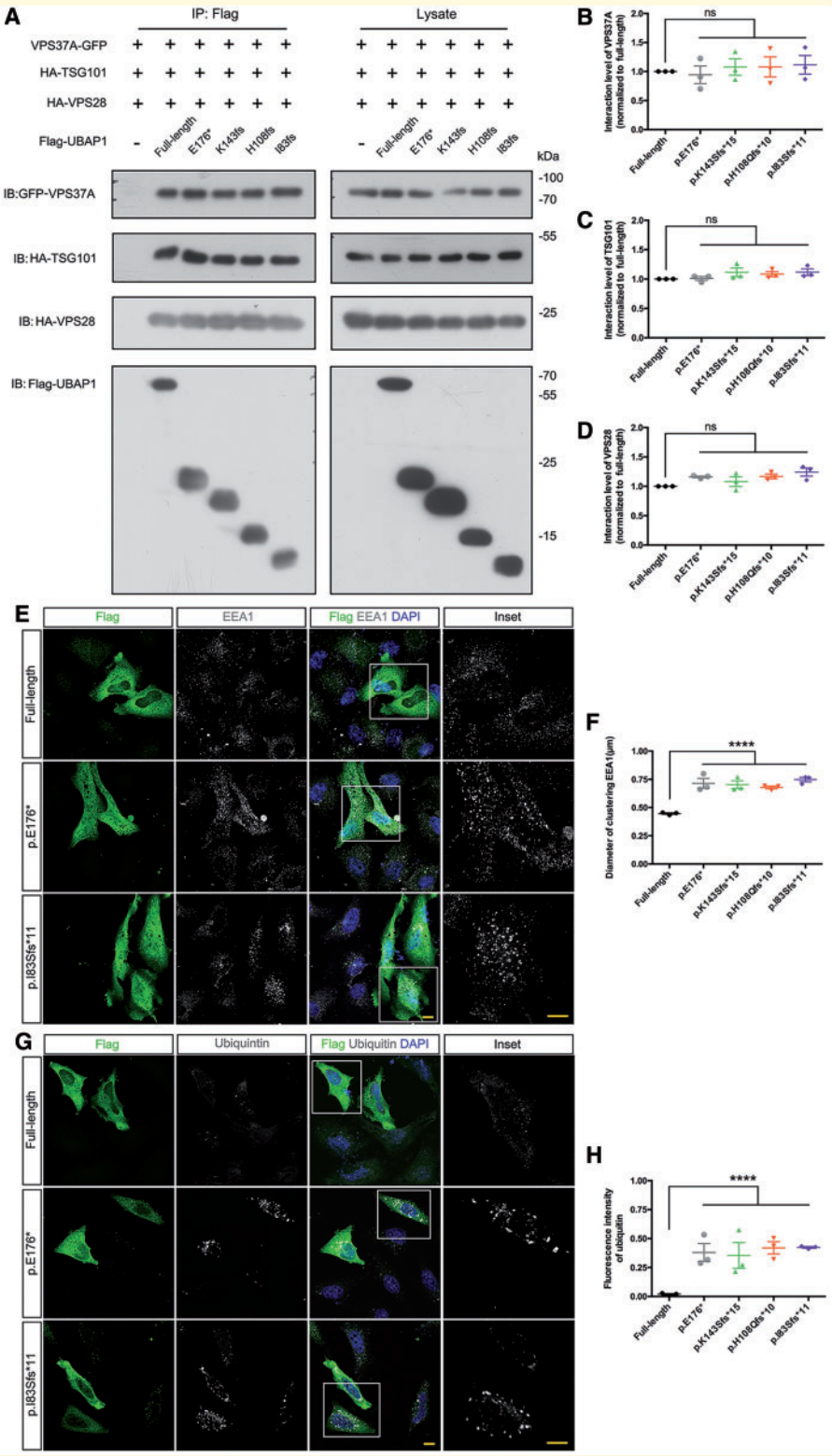

Figure 3 Truncation of UBAP1 impairs endosome processing and ubiquitin sorting but does not impair UBAP1's physical interaction with other ESCRT-I subunits. (**A**) Co-immunoprecipitation assays of the interactions of UBAP1 with other subunits of the ESCRT-I complex (VPS37A, TSG101 and VPS28). (**B**–**D**) Quantification the interaction level of VPS37A (**B**), TSG101 (**C**), and VPS28 (**D**) (n = 3). (**E** and **G**) Flag-tagged full-length human and a Flag-tagged truncation mutant UBAP1 variant were overexpressed in HeLa cells, followed by co-staining with an anti-Flag (green) and either an antibody against the early endosome marker EEA1(**E**, grey) or an antibody against ubiquitin (**G**, grey). The enlarged images on the right are magnified views of the boxed regions ($\times$5.0 magnification). Scale bar = 10 μm. (**F** and **H**) Measurement of the early endosome diameters in **F** (**E**, n = 3, with ~25 cells examined per group) and quantification of the fluorescent ubiquitin signal in **H** (**G**, n = 3, with ~30 cells examined per group). Error bars indicate means ± SEM. ns = not significant; ****$P < 0.0001$; one-way ANOVA.

region and the SOUBA domain, confocal microscopy and immunocytochemical staining for (i) the early endosome marker EEA1; (ii) ubiquitin; (iii) an EGFP-tagged form of UBAP1; and (iv) the nuclear marker DAPI revealed the conspicuous presence of aberrant endosome clustering, pronounced endosome enlargement, and cytoplasmic accumulation of ubiquitinated proteins in the truncation mutant cells (Fig. 3E, G and Supplementary Fig. 4). Specifically, compared to the full-length UBAP1, the truncation mutants had increased endosome clustering of 52–68% (Fig. 3F), and showed an 18–21-fold increase in accumulated ubiquitinated proteins (Fig. 3H). Taken together, our results collectively suggest that the mutations identified in the four HSP families apparently can disrupt the wild-type allele's function in early endosome processing and/or the sorting of ubiquitinated proteins.

Deletion of *Ubap1* impairs endosomal ubiquitin processing and promotes neurodegeneration

Given that pyramidal neurons in the corticospinal tract are known to be altered during the progression of HSP (Deluca *et al.*, 2004), we adopted an experimental strategy seeking to examine the effects of murine *Ubap1* knockout on endosome processing in *in vitro* cultured cortical mouse neurons. However, the Wellcome Sanger Institute reported that homozygous *Ubap1* mutation resulted in complete lethality by postnatal Day 14 (personal communication, Dr Ed Ryder). In light of the autosomal dominant inheritance by patients and the effects of UBAP1 mutant variants overexpression in HeLa cells, we thus proposed a dominant-negative pathomechanism for the stop-gain mutations. This hypothesis was supported by the normal appearance of the heterozygous *Ubap1* knockout mice (haploinsufficiency). To test our idea, we used a CRISPR/Cas9-based conditional knockout strategy to generate mice harbouring a Cre-inducible loxP-*Ubap1*-loxP construct, and confirmed the genotypes of homozygous $Ubap1^{flox/flox}$ mice (Fig. 4A). Note that to obtain the complete conditional knockout mice, we later crossed these mice with heterozygous $Ubap1^{flox}$; Cre^{NEX} and found that none of the surviving pups (or those that died soon after birth) were of the homozygous $Ubap1^{flox/flox}$; Cre^{NEX} genotype (Supplementary Fig. 5).

We thus performed surgery to extract cortical neurons from wild-type and homozygous $Ubap1^{flox/flox}$ mice and, prior to plating, we co-electrotransfected these neurons with a plasmid bearing an EEA1-Flag (to label early endosomes inside neuron cells, which is not possible with the aforementioned anti-EEA1 antibody), and a plasmid bearing a Cre-T2A-EGFP construct or CAG-EGFP construct. We then performed immunoblotting with an antibody that recognizes both human and mouse UBAP1, which confirmed the successful knockout of UBAP1 in the cultured $Ubap1^{flox/flox}$ neurons with Cre-directed recombination (Fig. 4B); note that no reduction in the UBAP1 protein level occurred in $Ubap1^{flox/flox}$ neurons lacking Cre treatment. Consistent with our findings in HeLa cells, confocal microscopy of immunocytochemical staining for EEA1-Flag or ubiquitin separately in *Ubap1* deletion neurons revealed obvious clustering of early endosomes and dramatically higher cytoplasmic levels of endosomal ubiquitinated proteins (by Day 3 of the *in vitro* cultures) (Fig. 4C–F); the same phenotypes were also observed in a longer, 12-day time course (Supplementary Fig. 6). $Ubap1^{flox/flox}$ neurons lacking Cre treatment had similarly low levels of inclusion bodies and ubiquitinated proteins as the wild-type neurons. Notably, we observed swelling, a common neurodegenerative disease phenotype (Chen *et al.*, 2014; Xu *et al.*, 2016), in some of the distal axonal regions of *Ubap1* deletion neurons, which co-localized with extensive endosome clustering and pronounced ubiquitinated protein accumulation (Fig. 4G–I).

Having determined that deletion of *Ubap1* disrupts both normal endosome processing and the sorting of ubiquitinated proteins (likely endosome cargoes) in corticospinal tract neurons, and considering that apoptosis is known to be involved in the progression of some HSP subtypes (Lee *et al.*, 2017; Denton *et al.*, 2018; Maruyama *et al.*, 2018), we next conducted experiments with cultured neurons and examined the presence of the apoptosis-related markers procaspase3 and activated caspase-3 and used terminal deoxynucleotidyl transferase (TdT)-mediated dUTP nick-end labelling (TUNEL) assays to examine if *Ubap1* deletion increased the extent of apoptosis in neurons cultured from the $Ubap1^{flox/flox}$ mice. Assessment at Day 5 of the *in vitro* cultures revealed that apoptosis was occurring in both wild-type and *Ubap1* deletion neurons, but showed that the extent of apoptosis was significantly increased in neurons with *Ubap1* knocked out (Fig. 4J–M and Supplementary Fig. 7A and B). We also counted neurons in the *Ubap1* knocked out cultures: we found significantly fewer double positive Tau/EGFP labelled neurons in the *Ubap1* deletion samples than in either the wild-type or $Ubap1^{flox/flox}$ controls in the absence of Cre samples (Supplementary Fig. 7C and D), further supporting our observation of neuronal loss. These results from mammalian neurons showing that deletion of *Ubap1* results in disrupted endosome and ubiquitinated protein processing as well as in increased apoptosis collectively provide preliminary evidence at the cellular mechanistic level that can potentially explain how the *UBAP1* mutations we observed in four HSP families may drive the pathogenesis of a previously unknown subtype of the neurodegenerative disease HSP.

Full-length, not truncated, human UBAP1 can rescue dysfunctional endosomal ubiquitin processing

We next conducted experiments to determine whether various forms of human UBAP1 can rescue the dysfunctional

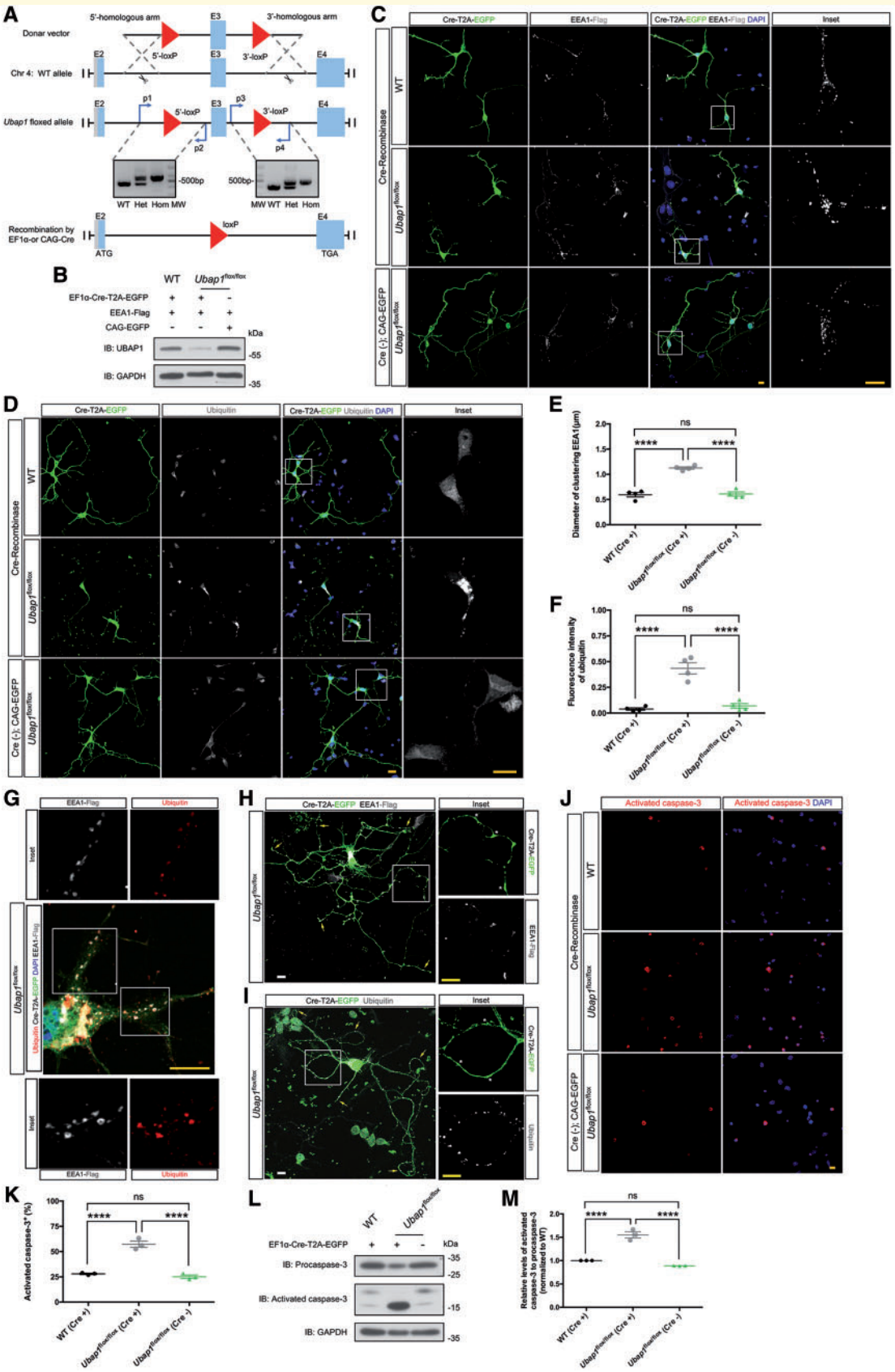

Figure 4 Deletion of *Ubap1* in mouse-derived cortical neurons impairs both endosomal processing and the sorting ubiquitinated proteins and promotes neurodegeneration. (**A**) Targeting strategy for the conditional deletion of *Ubap1*. Two loxP sites were inserted surrounding the genomic locus of *Ubap1* exon 3 via homologous recombination. Agarose gel image shows successful PCR amplification of

(continued)

endosomal processing phenotypes from deletion of *Ubap1* neurons. We prepared *in vitro* cortical neurons from homozygous *Ubap1*$^{flox/flox}$ mice, with one of three additional overexpression plasmids for: (i) full-length human UBAP1 (UBAP1$^{full\text{-}length}$); (ii) the HSP Family 3 truncated mutant variant of UBAP1^{K143fs}; or (iii) the control construct CAG-EGFP. Transfection efficiency was comparable (25 ~ 29%) for all constructs (Supplementary Fig. 8). Moreover, we also transfected wild-type neurons with plasmids for UBAP1$^{full\text{-}length}$ or UBAP1^{K143fs} (Supplementary Fig. 9). To enable visualization of endosomal processing, we also co-electrotransfected these neurons with a plasmid for EEA1-Flag expression.

Confocal microscopy with immunocytochemical staining for EEA1-Flag on culture Day 5 revealed that, whereas the full-length human UBAP1 was able to rescue the *Ubap1* deletion early endosome clustering phenotype. However, transgenic overexpression of the UBAP1 variant lacking its HD-PTP binding region and its SOUBA domain could not rescue this dysregulated endosomal processing (Fig. 5A and C). The extent of this rescue was evident in our finding that similarly low levels of inclusion bodies were present in wild-type neurons and *Ubap1* deletion neurons expressing full-length UBAP1. Consistent with all of our previous observations for the co-occurrence of the endosome clustering phenotype and increased accumulation of ubiquitinated proteins, staining of these *Ubap1*-deletion neurons with an anti-ubiquitin antibody revealed dramatically stronger ubiquitin signals in cells expressing the truncated UBAP1^{K143fs} variant as compared with the UBAP1$^{full\text{-}length}$ (Fig. 5B and D). Thus, our findings that a truncated mutant form of UBAP1 identified from an HSP patient is unable to rescue dysfunctional endosome processing and aberrant sorting of ubiquitinated proteins demonstrate that UBAP1's HD-PTP binding region and SOUBA domain are required for UBAP1's function in regulating endosomal ubiquitin sorting in mammalian neurons. Moreover, overexpression of UBAP1^{K143fs} in wild-type neurons caused aberrant endosome clustering, pronounced endosome enlargement, and cytoplasmic accumulation of ubiquitinated proteins, while overexpression of UBAP1$^{full\text{-}length}$ in wild-type neurons did not (Supplementary Fig. 9). Together, these results support that the UBAP1^{K143fs} protein exerts dominant-negative effects in cells, apparently conferring its toxicity via its promotion of inclusion body formation.

Discussion

UBAP1 was originally cloned as a tumour suppressor locus located at human chromosome 9p21–22 (Qian *et al.*, 2011). Notably, a previous linkage analysis reported *UBAP1* as a genetic risk factor for dementia (frontotemporal lobar degeneration, FTLD) (Rollinson *et al.*, 2009), and although we observed no obvious cognitive symptoms in these patients, monitoring for this condition while screening for *UBAP1* mutation is warranted.

The UBAP1 protein was shown to be a subunit of the mammalian ESCRT-I complex (Stefani *et al.*, 2011; Agromayor *et al.*, 2012). In yeast, ESCRTs are essential for several cellular processes including trafficking and sorting of proteins to the vacuole, cytokinesis, retroviral budding, and mRNA transport (Peel *et al.*, 2011; Hanson *et al.*, 2012). Of the four known human multi-protein ESCRTs, the heterotetrameric ESCRT-I complex is known to directly interact with other ESCRTs and, as described above, chaperones ubiquitinated cargo into MVBs (Raiborg and Stenmark, 2009; Shields and Piper, 2011).

The ESCRT-I complex can be formed by different isoforms of some subunits, and both UBAP1 and MVB12 have been observed as ESCRT-I subunits in cells (de Souza and Aravind, 2010; Stefani *et al.*, 2011; Agromayor *et al.*, 2012). Considering that the UBAP1 C-terminal SOUBA domain interacts with the cargo (Agromayor *et al.*, 2012), and in light of our finding that the HSP-inducing truncated *UBAP1* gene products created retain their ability to physically interact with other ESCRT-

Figure 4 Continued
detecting the 5′- and 3′-loxP sites. Upon Cre-directed recombination, the exon 3 can be excised to result in a premature stop codon (TGA) in the 5′ end of Exon 4. (**B**) Cortical neurons from wild-type (WT) and *Ubap1*$^{flox/flox}$ mice were co-electrotransfected with plasmids for Cre-T2A-EGFP and EEA1-Flag, and neurons in the absence of Cre as a control, followed by immunoblotting with an antibody against UBAP1. The full-length UBAP1 protein is Cre-dependent. (**C** and **D**) The neurons were fixed at culture Day 3, and co-stained with antibodies against EGFP (green) and either Flag (grey, **C**) or ubiquitin (grey, **D**). The enlarged images on the right are magnified views of the boxed regions (×5 magnification). Scale bar = 10 μm. (**E** and **F**) Measurement of the early endosome diameters in **E** (**C**, $n = 4$, with ~30 cells examined per group) and quantification of the fluorescent ubiquitin signal in **F** (**D**, $n = 4$, with ~40 cells examined per group). (**G**) Immunocytochemical staining analysis showed that clustered early endosomes were co-localized with accumulated ubiquitinated protein. (**H** and **I**) Clustering of early endosomes (**H**) and accumulation of ubiquitinated protein (**I**) was widespread throughout distal neurites (yellow arrows); note the especially strong EEA1 and ubiquitin signals at the regions with focal beading (white asterisks). The enlarged images on the right are magnified views of the boxed regions (×6 magnification). Scale bar = 10 μm. (**J** and **K**) Fluorescence microscopy of immunostained neuron cultures with activated caspase-3 (red) and DAPI (blue) revealed that *Ubap1*$^{flox/flox}$ neurons transfected with Cre exhibit significantly more apoptosis than wild-type or *Ubap1*$^{flox/flox}$ controls in the absence of Cre on DIV (days *in vitro*) 5 ($n = 3$). (**L** and **M**) Immunoblots of procaspase-3 and activated caspase-3 in neuron culture revealed that Cre-transfected *Ubap1*$^{flox/flox}$ neurons exhibited significantly higher levels of apoptosis than wild-type or *Ubap1*$^{flox/flox}$ controls in the absence of Cre on DIV 5 ($n = 3$). Error bars indicate means ± SEM. ns = not significant; ****$P < 0.0001$, one-way ANOVA.

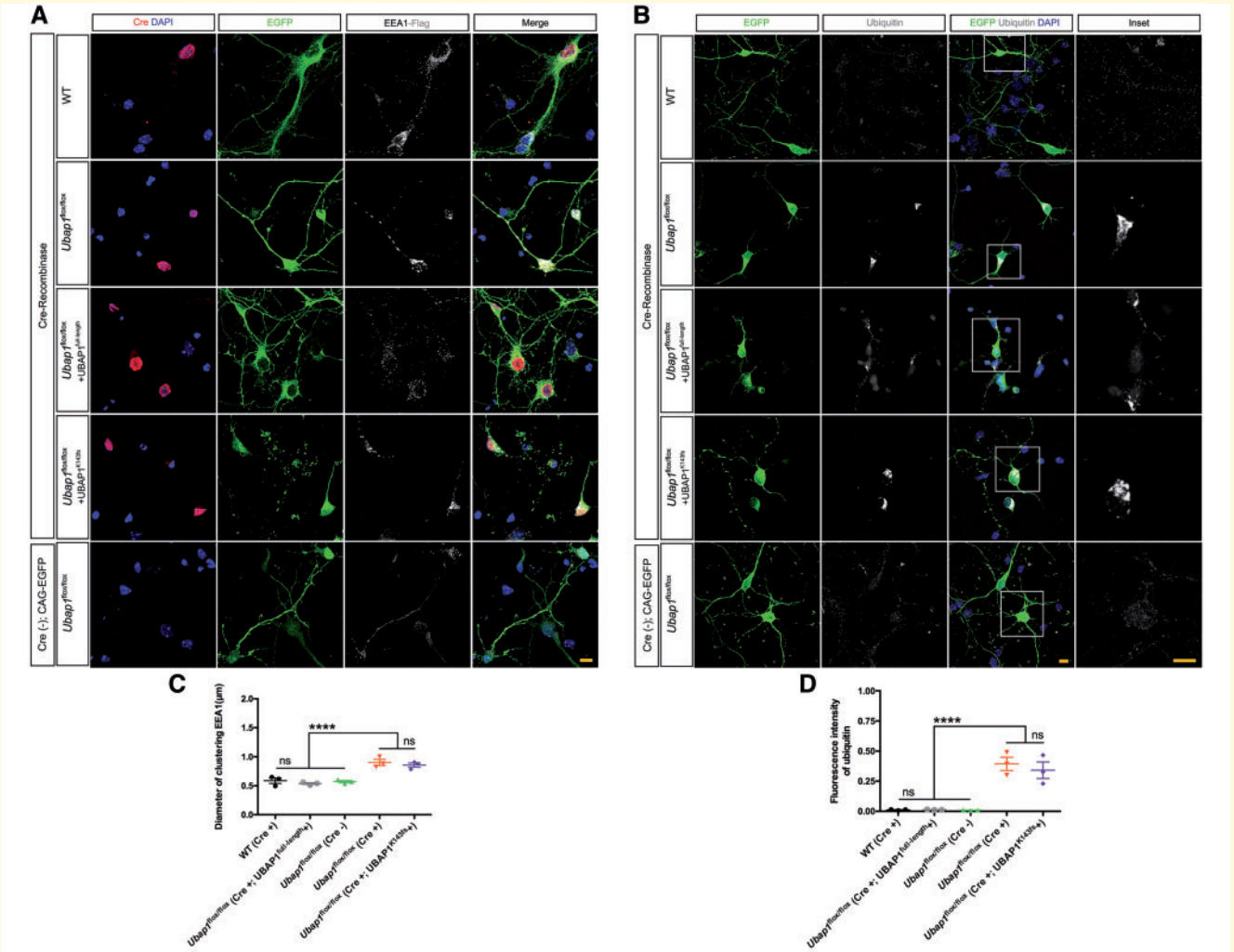

Figure 5 Full-length human UBAP1 but not truncated UBAP1 can rescue the impaired endosomal processing and ubiquitinated protein sorting phenotypes of murine *Ubap1*-deletion cortical neurons. (**A**) Confocal fluorescence microscopy of early processing in endosomes. Neurons were fixed at culture Day 5 and were co-stained with antibodies against Cre (red), DAPI (blue), EGFP (green) and Flag (grey). (**B**) Analysis of ubiquitinated protein sorting. Neurons were fixed at Day 5 and were co-stained with EGFP (green), ubiquitin (grey) and DAPI (blue). The enlarged images on the right are magnified views of the boxed regions (×5 magnification). Scale bar = 10 μm. (**C**) Measurement of the diameter of early endosomes of **C** (**A**, $n = 3$, with ~25 cells examined per group). (**D**) Quantification of the fluorescent ubiquitin signal in **D** (**B**, $n = 3$, with ~30 cells examined per group). Error bars indicate means ± SEM. ns = not significant; ****$P < 0.0001$; one-way ANOVA.

I subunits, we speculate that the stop-gain mutations specifically disrupt UBAP1's binding to ubiquitinated proteins.

Importantly, previous work showed that mutations of *VPS37A*—one of four VPS37 splicing variants expressed in mammalian cells (Bache *et al.*, 2004)—are associated with a form of complicated HSP (Zivony-Elboum *et al.*, 2012). The core neuropathology of HSP is the axonal degeneration of corticospinal tracts and fasciculus gracilis (Wharton *et al.*, 2003; Deluca *et al.*, 2004). Axonal degeneration is the initial pathological mechanism in many degenerative neurological diseases, and in HSP this degeneration principally involves a so-called 'dying-back' (i.e. axon-then-soma) of the longest descending corticospinal axons (Deluca *et al.*, 2004; Blackstone, 2012). Our observations of swollen axons in the distal regions of cultured cortical neurons is consistent with prior characterization of dying back and with a role for UBAP1 in HSP neurodegeneration. Neurite swelling occurs in motor neurons in disorders including ALS and spinal muscular atrophy (Chen *et al.*, 2014; Xu *et al.*, 2016); one possible explanation for the observed swelling could be an excess of unprocessed endosomes and/or cargo.

Selective interaction of UBAP1 with ESCRT-I complexes containing the VPS37A isoform has been reported (Stefani *et al.*, 2011; Agromayor *et al.*, 2012; Wunderley *et al.*, 2014). Thus, ESCRT-I dysfunction induced by mutations in *UBAP1* or *VPS37A* may commonly entail HSP pathogenesis. Given that abnormal endocytic trafficking occurs in several neurodegenerative disorders (e.g. Alzheimer's disease, Down syndrome, and Parkinson's disease) (Wang

et al., 2014), it follows that disruption of function for the endosome-lysosomal pathway for intracellular trafficking contributes to disease by preventing the clearance of misfolded proteins (Hu *et al.*, 2015; Song *et al.*, 2016). For example, the epidermal growth factor receptor and tropomyosin-related kinase receptor are both known to be involved in neurodegeneration (Pankratova *et al.*, 2018; Sadanand *et al.*, 2018). Normal endosomal sorting and trafficking are required for the deposition of these receptors into the membranes of healthy neurons, thus suggesting that dysfunction in endosomal processing, trafficking, and removal of ubiquitinated proteins in HSP patients carrying mutated alleles of *UBAP1*, may subsequently cause neuropathological defects in endocytosis and vesicle trafficking.

Previous studies have shown that siRNA-mediated knockdown of UBAP1 results in (i) the accumulation of ubiquitinated proteins in endosomes; and (ii) the obstruction of lysosomal degradation (Agromayor *et al.*, 2012; Gahloth *et al.*, 2016). Consistent with these findings, we showed that deletion of *Ubap1* caused early endosomes to cluster together with concurrent accumulation of ubiquitinated proteins, potentially promoting neurodegenerative pathogenesis. We here provide preliminary evidence supporting the involvement of apoptosis in this neurodegeneration, though possibly other forms of programmed cell death (e.g. necroptosis) are involved (Oshima *et al.*, 2016).

Future studies examining the cellular dynamics of vesicle processing, the sorting and degradation of ubiquitinated proteins, as well as observations about the distribution of full-length (or truncated) UBAP1 and other ESCRT-1 subunits in the nervous systems of disease specimens (e.g. patient fibroblasts or skin/nerve biopsy) will likely deepen our understanding of how the genetic variations we identified in HSP families ultimately cause HSP and perhaps other neurodegenerative diseases. HSP is a relatively common neurodegenerative disorder, and our identification and characterization of a new *UBAP1*-driven HSP subtype represents an important step forward towards developing a comprehensive understanding of the molecular basis of this disease.

Acknowledgements

We sincerely thank the patients and their relatives for participation. In addition, Xiang Lin wants to thank the patience, care and support from Liu-Qing Hong over the past years.

Funding

This work was supported by grants 81771230 (W.-J.C.), 81801130 (X.L.), and U1505222 (N.W.) from the National Natural Science Foundation of China, and by Joint Funds for the Innovation of Science and Technology of Fujian Province (2017Y9094) (W.-J.C.), the National Key Clinical Specialty Discipline Construction Program (N.W.), and the Key Clinical Specialty Discipline Construction Program of Fujian (N.W.).

Competing interests

The authors report no competing interests.

Supplementary material

Supplementary material is available at *Brain* online.

References

Agromayor M, Soler N, Caballe A, Kueck T, Freund SM, Allen MD, et al. The UBAP1 subunit of ESCRT-I interacts with ubiquitin via a SOUBA domain. Structure 2012; 20: 414–28.

Bache KG, Slagsvold T, Cabezas A, Rosendal KR, Raiborg C, Stenmark H. The growth-regulatory protein HCRP1/hVps37A is a subunit of mammalian ESCRT-I and mediates receptor down-regulation. Mol Biol Cell 2004; 15: 4337–46.

Blackstone C. Cellular pathways of hereditary spastic paraplegia. Annu Rev Neurosci 2012; 35: 25–47.

Chen H, Qian K, Du Z, Cao J, Petersen A, Liu H, et al. Modeling ALS with iPSCs reveals that mutant SOD1 misregulates neurofilament balance in motorneurons. Cell Stem Cell 2014; 14: 796–809.

Coutelier M, Goizet C, Durr A, Habarou F, Morais S, Dionne-Laporte A, et al. Alteration of ornithine metabolism leads to dominant and recessive hereditary spastic paraplegia. Brain 2015; 138: 2191–205.

Deluca GC, Ebers GC, Esiri MM. The extent of axonal loss in the long tracts in hereditary spastic paraplegia. Neuropathol Appl Neurobiol 2004; 30: 576–84.

de Souza RF, Aravind L. UMA and MABP domains throw light on receptor endocytosis and selection of endosomal cargoes. Bioinformatics 2010; 26: 1477–80.

Denton K, Mou Y, Xu CC, Shah D, Chang J, Blackstone C, et al. Impaired mitochondrial dynamics underlie axonal defects in hereditary spastic paraplegias. Hum Mol Genet 2018; 27: 2517–30.

Dong EL, Wang C, Wu S, Lu YQ, Lin XH, Su HZ, et al. Clinical spectrum and genetic landscape for hereditary spastic paraplegias in China. Mol Neurodegener 2018; 3: 36.

Estrada-Cuzcano A, Martin S, Chamova T, Synofzik M, Timmann D, Holemans T, et al. Loss-of-function mutations in the ATP13A2/PARK9 gene cause complicated hereditary spastic paraplegia (SPG78). Brain 2017; 140: 287–305.

Fink JK. Hereditary spastic paraplegia: clinico-pathologic features and emerging molecular mechanisms. Acta Neuropathol 2013; 126: 307–28.

Gahloth D, Levy C, Heaven G, Stefani F, Wunderley L, Mould P, et al. Structural basis for selective interaction between the ESCRT regulator HD-PTP and UBAP1. Structure 2016; 24: 2115–26.

Hanson PI, Cashikar A. Multivesicular body morphogenesis. Annu Rev Cell Dev Biol 2012; 28: 337–62.

Harding AE. Classification of the hereditary ataxias and paraplegias. Lancet 1983; 1: 1151–5.

Hu YB, Dammer EB, Ren RJ, Wang G. The endosomal-lysosomal system: from acidification and cargo sorting to neurodegeneration. Transl Neurodegener 2015; 4: 18.

Jardin N, Giudicelli F, Ten Martín D, Vitrac A, De Gois S, Allison R, et al. BMP- and neuropilin 1-mediated motor axon navigation relies on spastin alternative translation. Development 2018; 145: dev162701.

Kanungo J, Lantz S, Paule MG. In vivo imaging and quantitative analysis of changes in axon length using transgenic zebrafish embryos. Neurotoxicol Teratol 2011; 33: 618–23.
Kara E, Tucci A, Manzoni C, Lynch DS, Elpidorou M, Bettencourt C, et al. Genetic and phenotypic characterization of complex hereditary spastic paraplegia. Brain 2016; 139: 1904–18.
Kozol RA, Abrams AJ, James DM, Buglo E, Yan Q, Dallman JE. Function over form: modeling groups of inherited neurological conditions in zebrafish. Front Mol Neurosci 2016; 9: 55.
Kruglyak L, Daly MJ, Reeve-Daly MP, Lander ES. Parametric and nonparametric linkage analysis: a unified multipoint approach. Am J Hum Genet 1996; 58: 1347–63.
Lee JA, Gao FB. Neuronal Functions of ESCRTs. Exp Neurobiol 2012; 21: 9–15.
Lee JYW, Hsu CK, Michael M, Nanda A, Liu L, McMillan JR, et al. Large intragenic deletion in DSTYK underlies autosomal-recessive complicated spastic paraparesis, SPG23. Am J Hum Genet 2017; 100: 364–70.
Lo Giudice T, Lombardi F, Santorelli FM, Kawarai T, Orlacchio A. Hereditary spastic paraplegia: clinical-genetic characteristics and evolving molecular mechanisms. Exp Neurol 2014; 261: 518–39.
Loncle N, Agromayor M, Martin-Serrano J, Williams DW. An ESCRT module is required for neuron pruning. Sci Rep 2015; 5: 8461.
Martin E, Schüle R, Smets K, Rastetter A, Boukhris A, Loureiro JL, et al. Loss of function of glucocerebrosidase GBA2 is responsible for motor neuron defects in hereditary spastic paraplegia. Am J Hum Genet 2013; 92: 238–44.
Maruyama T, Maruyama T, Baba T, Maemoto Y, Hara-Miyauchi C, Hasegawa-Ogawa M, et al. Loss of DDHD2, whose mutation causes spastic paraplegia, promotes reactive oxygen species generation and apoptosis. Cell Death Dis 2018; 9: 797.
Ohki Y, Wenninger-Weinzierl A, Hruscha A, Asakawa K, Kawakami K, Haass C, et al. Glycine-alanine dipeptide repeat protein contributes to toxicity in a zebrafish model of C9orf72 associated neurodegeneration. Mol Neurodegener 2017; 12: 6.
Oshima R, Hasegawa T, Tamai K, Sugeno N, Yoshida S, Kobayashi J, et al. ESCRT-0 dysfunction compromises autophagic degradation of protein aggregates and facilitates ER stress-mediated neurodegeneration via apoptotic and necroptotic pathways. Sci Rep 2016; 6: 24997.
Pankratova S, Klingelhofer J, Dmytriyeva O, Owczarek S, Renziehausen A, Syed N, et al. The S100A4 protein signals through the ErbB4 receptor to promote neuronal survival. Theranostics 2018; 8: 3977–90.
Parkinson N, Ince PG, Smith MO, Highley R, Skibinski G, Andersen PM, et al. ALS phenotypes with mutations in CHMP2B (charged multivesicular body protein 2B). Neurology 2006; 67: 1074–7.
Peel S, Macheboeuf P, Martinelli N, Weissenhorn W. Divergent pathways lead to ESCRT-III-catalyzed membrane fission. Trends Biochem Sci 2011; 36: 199–210.
Qian J, Yang J, Zhang X, Zhang B, Wang J, Zhou M, et al. Isolation and characterization of a novel cDNA, UBAP1, derived from the tumor suppressor locus in human chromosome 9p21–22. J Cancer Res Clin Oncol 2011; 127: 613–18.
Raiborg C, Stenmark H. The ESCRT machinery in endosomal sorting of ubiquitylated membrane proteins. Nature 2009; 458: 445–52.
Richards S, Aziz N, Bale S, Bick D, Das S, Gastier-Foster J, et al. Standards and guidelines for the interpretation of sequence variants: a joint consensus recommendation of the American College of Medical Genetics and Genomics and the Association for Molecular Pathology. Genet Med 2015; 17: 405–24.
Rollinson S, Rollinson S, Rizzu P, Sikkink S, Baker M, Halliwell N, et al. Ubiquitin associated protein 1 is a risk factor for frontotemporal lobar degeneration. Neurobiol Aging 2009; 30: 656–65.
Ruano L, Melo C, Silva MC, Coutinho P. The global epidemiology of hereditary ataxia and spastic paraplegia: a systematic review of prevalence studies. Neuroepidemiology 2014; 42: 174–83.
Sadanand A, Sadanand A, Janardhanan A, Vanisree AJ, Pavai T. Neurotrophin expression in lymphocytes: a powerful indicator of degeneration in Parkinson's disease, amyotrophic lateral sclerosis and ataxia. J Mol Neurosci 2018; 64: 224–32.
Sheehan P, Zhu M, Beskow A, Vollmer C, Waites CL. Activity-dependent degradation of synaptic vesicle proteins requires Rab35 and the ESCRT pathway. J Neurosci 2016; 36: 8668–86.
Shields SB, Piper RC. How ubiquitin functions with ESCRTs. Traffic 2011; 12: 1306–17.
Skibinski G, Parkinson NJ, Brown JM, Chakrabarti L, Lloyd SL, Hummerich H, et al. Mutations in the endosomal ESCRTIII-complex subunit CHMP2B in frontotemporal dementia. Nat Genet 2005; 37: 806–8.
Söllvander S, Nikitidou E, Brolin R, Söderberg L, Sehlin D, Lannfelt L, et al. Accumulation of amyloid-β by astrocytes result in enlarged endosomes and microvesicle-induced apoptosis of neurons. Mol Neurodegener 2016; 11: 38.
Song P, Trajkovic K, Tsunemi T, Krainc D. Parkin modulates endosomal organization and function of the endo-lysosomal pathway. J Neurosci 2016; 36: 2425–37.
Song Y, Wang M, Mao F, Shao M, Zhao B, Song Z, et al. Knockdown of Pnpla6 protein results in motor neuron defects in zebrafish. Dis Model Mech 2013; 6: 404–13.
Stefani F, Zhang L, Taylor S, Donovan J, Rollinson S, Doyotte A, et al. UBAP1 is a component of an endosome-specific ESCRT-I complex that is essential for MVB sorting. Curr Biol 2011; 21: 1245–50.
Sweeney NT, Brenman JE, Jan YN, Gao FB. The coiled-coil protein shrub controls neuronal morphogenesis in Drosophila. Curr Biol 2006; 16: 1006–11.
Wang X, Huang T, Bu G, Xu H. Dysregulation of protein trafficking in neurodegeneration. Mol Neurodegener 2014; 9: 31.
Wharton SB, McDermott CJ, Grierson AJ, Wood JD, Gelsthorpe C, Ince PG, et al. The cellular and molecular pathology of the motor system in hereditary spastic paraparesis due to mutation of the spastin gene. J Neuropathol Exp Neurol 2003; 62: 1166–77.
Wunderley L, Brownhill K, Stefani F, Tabernero L, Woodman P. The molecular basis for selective assembly of the UBAP1-containing endosome-specific ESCRT-I complex. J Cell Sci 2014; 127: 663–72.
Xu CC, Denton KR, Wang ZB, Zhang X, Li XJ. Abnormal mitochondrial transport and morphology as early pathological changes in human models of spinal muscular atrophy. Dis Model Mech 2016; 9: 39–49.
Zempel H, Mandelkow EM. Tau missorting and spastin-induced microtubule disruption in neurodegeneration: Alzheimer disease and hereditary spastic paraplegia. Mol Neurodegener 2015; 10: 68.
Zivony-Elboum Y, Westbroek W, Kfir N, Savitzki D, Shoval Y, Bloom A, et al. A founder mutation in Vps37A causes autosomal recessive complex hereditary spastic paraparesis. J Med Genet 2012; 49: 462–72.